Surface & Coatings Technology 270 (2015) 284–289

Contents lists available at ScienceDirect

Surface & Coatings Technology

journal homepage: www.elsevier.com/locate/surfcoat

Enhancement of biocorrosion resistance of epoxy coating by addition of Ag/Zn exchanged a zeolite

Andrea M. Pereyra [a,b], Maximiliano R. Gonzalez [b], Thais A. Rodrigues [c], Marcia T. Soares Luterbach [c], Elena I. Basaldella [a,b,*]

[a] CITEMA, Universidad Tecnológica Nacional, Facultad Regional La Plata, 60 y 124, 1900 La Plata, Argentina
[b] CINDECA, CCT-La Plata-CONICET, Universidad Nacional de La Plata, 47N 257 (B1900AJK), La Plata, Argentina
[c] LABIO-INT/MCT, Av. Venezuela 82, Rio de Janeiro, RJ 20081-310, Brazil

ARTICLE INFO

Article history:
Received 6 October 2014
Accepted in revised form 22 February 2015
Available online 28 February 2015

Keywords:
Biofilms
Biocidal cations
Epoxy coating
Pseudomonas aeruginosa
Zeolites

ABSTRACT

The incorporation of a synthetic zeolite containing biocide cations in epoxy formulations to prevent biofilm formation and the biodegradation processes derived from its presence was studied. Biocidal action of Ag/Zn-exchanged A type zeolite against *Pseudomonas aeruginosa*, bacteria usually found in fluid containers from the oil refining industry, was determined by microbiological evaluation using molecular biology and traditional cultivation techniques. The minimum inhibitory concentration method (MIC) was adopted to assess the effect of Ag^{+1} and Zn^{+2} impregnated zeolites on microorganism growth. Cell quantification on biofilms detached from epoxy coated steel coupons indicate that *P. aeruginosa* cells contained in the biofilm significantly decreased as the zeolite percentage in the epoxy formulation was increased. An inhibitory effect of up to seven orders of magnitude was obtained when Ag/Zn-exchanged A zeolite having MIC value about 200 $mg \cdot L^{-1}$ was used as additive in epoxy coatings formulations.

1. Introduction

Microbiologically influenced corrosion and biofouling processes are mediated by microorganisms adhered to metal surfaces when embedded in a gelatinous matrix called biofilm. Microbial adhesion processes lead to an important modification of the metal/solution interface, generally increasing the aggressiveness of the medium against the substratum [1]. Microbiologically influenced corrosion and biofouling that affect industrial systems range from heavy microbiological contamination with consequent energy and efficiency losses to structural failures owing to corrosion [2].

With regard to corrosion in the oil industry, the implementation of control and treatment systems, and failure mitigation plans in each process stage (exploitation, transportation, production and storage) involves high costs. It is well known that the exploitation stage is critical, especially when the water/oil ratio is high. In these cases, corrosive water conditions, high temperatures and pressures, salinity, suspended solid concentration and bacteria present in the well provide sufficiently aggressive conditions to generate corrosion.

In the storage step, the most common problem is related to the proliferation of microorganisms. This process is promoted by the availability of several nutrients (water, moisture, oxygen, mineral additives). Thus, the growth of aerobic organisms with surfactant properties generates product contamination, which may lead to decreased quality, sludge formation, and deterioration of pipes, filters, valves, etc. [3].

Currently, the use of protective coatings is a methodology usually employed to provide effective control of microbiologically influenced corrosion. In the case of storage tanks, the protective interior topcoat is based on epoxy resin, which is generally improved with cathodic protection. Epoxy systems act as insulating barriers between steel and aggressive media. They are widely used due to an excellent combination of mechanical properties, chemical stability, corrosion and wear resistance as well as adhesiveness to most metals and alloys [4,5].

Furthermore, zeolites are crystalline aluminosilicate compounds that are classified according to common features of the framework structures. Particularly, NaA zeolite is a specific arrangement in which the unit cell contains 24 tetrahedra, 12 AlO_4 and 12 SiO_4. When fully hydrated, there are 27 water molecules per unit cell, and there is also one sodium cation for each framework aluminum. These sodium ions are rather loosely held, so one of the main uses of this material is based on its cation exchange properties. Thus, sodium ions are exchangeable by silver, copper or zinc ions to functionalize zeolites as antibacterial agents.

In the last years, efficacy in the uses of these materials in several technological and biomedical applications has been reported [6–13] and it has been observed that the use of metal-functionalized microporous materials as antimicrobial agents shows promising results.

In this paper, samples of NaA containing different quantities of Ag^{+1} and Zn^{+2} were prepared by cation exchange in order to evaluate their antibacterial properties. The biocide cations Ag^{+1} and Zn^{+2} were hosted

* Corresponding author at: CINDECA, CCT-La Plata-CONICET, Universidad Nacional de La Plata, 47N 257 (B1900AJK), La Plata, Argentina.

http://dx.doi.org/10.1016/j.surfcoat.2015.02.044
0257-8972/

in the cavities of the ordered aluminosiliceous framework. Minimum inhibitory concentration values corresponding to the exchanged zeolites and the antibacterial activity of these products against *Pseudomonas aeruginosa* after incorporation in an epoxy coating formulation used for steel protection were determined.

2. Experimental

2.1. Preparation of cation-exchanged zeolites

2.1.1. Materials

NaA, synthetized in our laboratory, with a theoretical ion exchange capacity of 7.04 mEq·g^{-1} (unhydrated base) and of 5.48 mEq·g^{-1} (hydrated base) was used. Zeolite crystals were prepared by batch hydrothermal crystallization. The batch experiment was carried out in a closed polypropylene container, at 365 K, without stirring. The raw materials used were NaOH (Carlo Erba, analytical reagent), commercial sodium aluminate (36.5 wt.% Al_2O_3, 29.6 wt.% Na_2O, 33.9 wt.% H_2O) commercial water glass (9.2 wt.% Na_2O, 26.8 wt.% SiO_2, 64% wt% H_2O), and distilled water.

2.1.2. Ion-exchange experiments

The solution for the cation exchange was prepared with $AgNO_3$ (Carlo Erba, analytical reagent), $Zn(NO_3)_2$ (Carlo Erba, analytical reagent) and NH_4NO_3 (Carlo Erba, analytical reagent), using non-mineralized water as solvent. Ion exchange was carried out contacting 1 g of NaA with 1 L of the exchange solution under stirring. After a contact time of 3 h at 25 °C, the solid was separated from the liquid by filtration. The solid phase was dried in an oven at 60 °C and stabilized at room temperature and 35% relative humidity.

The liquid phase was analyzed by atomic absorption spectrometry (AAS) with a Varian AA220 model double beam spectrophotometer. The chemical composition of the zeolite products obtained, Ag/Zn-exchanged NaA (AgZnA), and the corresponding solution used for the exchange run are detailed in Table 1.

To evaluate any possible structural change, the synthesized zeolite NaA and the product after the cation exchange test were characterized by X-ray diffraction (XRD). The diffraction patterns were obtained with a Philips PW 1732/10 using Cu Kα radiation and a Ni filter at a rate of 2°/min. The diffraction diagram of the zeolite sample was identified by comparison with those detailed in the literature [14].

2.2. Minimum inhibitory concentration (MIC)

To evaluate the performance of AgZnA against *P. aeruginosa*, the minimum inhibitory concentration method was used. MIC is defined as the minimum concentration at which the agent takes the bacteria multiplication rate to zero. The *P. aeruginosa* used for these studies was isolated from the oil refining industry. The *P. aeruginosa* strain belongs to the Laboratório de Biocorrosão e Biodegradação — LABIO (Instituto Nacional de Tecnologia INT — MCTI), Rio de Janeiro, Brazil. Bacterial identification was performed by molecular biology-based methods/techniques. DNA from the pure strain was extracted using a commercial DNA isolation kit. After extraction, the bacterial 16S rRNA gene was amplified by PCR (technique of polymerase chain reaction) using the universal primer set SAdir (5′-AGAGTTTGATCATGGCTCAGA-3′, forward) and S17 Rev (5′GTTACCTTGTTACGACTT-3′, reverse). Sequencing of the 16S RNA gene was performed, followed by identification of phylogenetic strains using gene sequences obtained with those available in GenBank.

To evaluate the minimum inhibitory concentration of the biocidal cations supported on the zeolite, different metal concentrations were obtained by adding different weights of AgZnA to agar medium. Concentrations of 50 to 500 mg·L^{-1} were evaluated in Petri dishes. The starting NaA and a control sample without zeolite were also tested.

To ensure sterilization, zeolite powders were exposed to UV irradiation in a laminar flow chamber (Trox Mod. FLUCLII A1).

The agar medium supplemented with zeolite powder at the aforementioned concentrations was inoculated with 1 mL of the freshly prepared *P. aeruginosa* suspension (10^6 CFU·mL^{-1}). The microorganisms were seeded over the entire surface of the agar plate and then incubated for 48 h at 30 °C. Subsequently, bacterial growth was measured. All the experiments were carried out in triplicate. The results of these assays allowed obtaining the Ag^{+1}–Zn^{+2} concentrations supported on zeolite matrices required to inhibit microbiological growth.

2.3. Epoxy coating formulation and manufacture

Epoxy resin (specific weight, 1.280 kg·L^{-1}) was used as the epoxy matrix. The epoxy curing agent was a polyamide (specific weight, 0.980 kg·L^{-1}). Both products are from Steelcote, Argentina. AgZnA was added to the epoxy resin using a high-speed dispersion device (Alumcraft, Argentina, Model: AL 101). To prevent zeolite crystal agglomeration, a dispersant agent based on soya lecithin was employed. Subsequently, the curing agent was added to the resin (1/4 in/by volume) and dispersed for 60 min at 2800 rpm, ensuring laminar flow. Five epoxy coatings were prepared by varying the zeolite weight added. Coatings containing 0, 1, 4, 5 and 8 (%w/w) of AgZnA were prepared (coatings A, B, C, D and E, respectively). The coatings were applied by airless spray over metallic substrates (SAE 1010 steel coupons, 1 × 1 cm, grade A). The coupons were previously degreased with solvent in the vapor phase and then sanded to Sa 2 1/2° (SIS specification 05 59 00/67; maximum roughness R_m, 35 μm). Two coats of paints were applied on the thoroughly cleaned steel surfaces by means of an airless spray. The coated samples were left in the laboratory at 25 ± 2 °C for 7 days to ensure full drying and curing of the films. Steel coupons were prepared in triplicate for each test. In all samples the resulting dry film thickness measured using Fischer equipment was 110 ± 5.2 μm. Coating compositions are given in Table 2. For V-E coated coupon, surface and cross section were observed by SEM (scanning electron microscopy; Philips SEM 505). The cross section was obtained by cutting the coated coupons with a guillotine shear machine. The epoxy coatings were also characterized by Fourier transform infrared spectroscopy (FTIR). The FTIR analysis was performed in IRAffinity-1 Shimadzu equipment. For each spectrum, 48 scans were acquired at a spectra resolution of 4 cm^{-1}.

2.4. Microbiological corrosion assay

To ensure sterilization, prior to starting the test the coated coupons were exposed to UV irradiation during 15 min in a laminar flow chamber (Trox Mod. FLUCLII A1).

P. aeruginosa strain was grown in nutrient broth (yeast extract 2.0 g·L^{-1}; peptone 5.0 g·L^{-1}, sodium chloride 5.0 g·L^{-1} Oxoid Ltd.)

Table 1
Ag^{+1} and Zn^{+2} concentrations in the prepared material and composition of the corresponding aqueous solution used for cation exchange.

Sample	[Ag^{+1}] (%w/w)	Zn^{+2} (%w/w)	Exchange solution (mol·L^{-1})		
			[Ag^{+1}]	[Zn^{+2}]	[NH_4^{+1}]
AgZnA	5.4	6.0	0.127	0.309	0.787

Table 2
Coupon composition.

Coated coupon	Coating	[AgZnA] in epoxy coating (%w/w)	Average thickness measurement (μm)
I	A	0	105.9
II	B	1	107.1
III	C	4	111.3
IV	D	5	111.8
V	E	8	113.9

at 30 °C overnight. The cells of *P. aeruginosa* were centrifuged at 10,000 *g* for 10 min (Legend Mach 1.6R — Thermo Scientific Sorval®) and rinsed in saline to remove the culture medium. Cells were resuspended in Bushnell-Haas media. For contact experiments, coupons were placed face down in the culture (*P. aeruginosa* initial concentration, $>2.4 \times 10^{10}$ CFU·mL^{-1}) previously raised to a temperature of 30 °C and then incubated for 48 h. All experiments were carried out in triplicate. Following incubation, the coupons were removed from the Bushnell-Haas media and the biofilm was detached. Cell quantification on the biofilm was statistically measured by the technique of the Most Probable Number (MNP) [15].

3. Results and discussion

3.1. Zeolite characterization

XRD studies conducted on the starting NaA sample show the diffraction peaks corresponding to pure NaA zeolite. Signals were observed at 2θ = 7.2°, 10.2°, 12.5°, 16.1°, 21.7°, 24°, 27.1°, 29.9°, 34.2°, and 36.5° [14]. By comparing the diffraction patterns obtained for the zeolite material before and after ion exchange, it can be observed that NH_4^{+1}, Ag^{+1} and Zn^{+2} incorporation does not promote structural modifications. The XRD patterns obtained before and after cation exchange (Fig. 1) show no difference in the positions of the characteristic peaks associated with the presence of LTA structure, indicating that the network parameters are preserved and cation incorporation has not modified the crystalline arrangement. Differences about heights in diffraction peaks are due to the different natures of cations occupying cationic positions inside the zeolite structure. The diffraction peaks at about 2θ = 20 and 27° are assigned to the presence of [220] and [320] planes respectively [14]. Peaks corresponding to Zn or Ag compounds are not observed, probably due to low amounts of these species in the zeolite matrix, indicating that these metals are highly dispersed in the solid structure.

The relative crystallinity was estimated by measuring the height of two characteristic diffraction peaks of AgZnA and comparing those values to the corresponding heights measured in the pattern of the starting zeolite, which were set to be 100%. Using this method, the AgZnA zeolite crystallinity was about 80%. Nevertheless, these values should be considered as a semiquantitative estimation, because it is known that cation exchange may modify peak intensities [16]. In fact, after cation exchange, a significant change in the relative peak intensity can be observed (Fig. 1).

It is worthwhile to note that NH_4^{+1} cation should also be present in the zeolite structure occupying some exchange cation positions. Nevertheless, NH_4^{+1} was not considered as having biocidal activity, and it is used in this case to contribute to manage Ag^{+1} and Zn^{+2} incorporation.

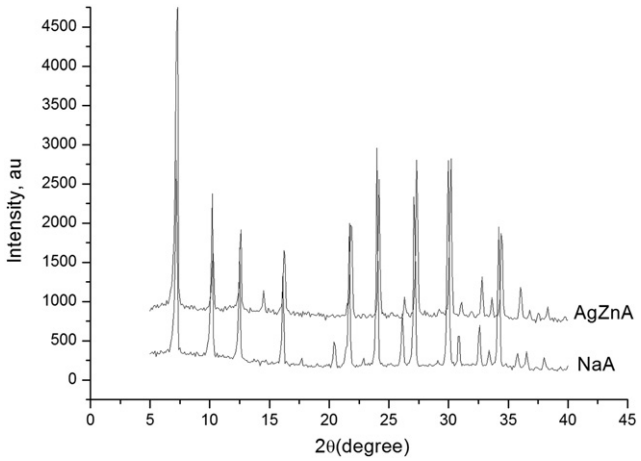

Fig. 1. XRD spectra for NaA and AgZnA zeolites.

The FTIR spectra of NaA, AgZnA and the nitrate salts (NH_4NO_3, $AgNO_3$ and $Zn(NO_3)_2$) are presented in Fig. 2a and b, respectively. Samples were dehydrated at 100 °C for 24 h and then prepared by the standard KBr pellet method. KBr was dried at 200 °C for 24 h [17].

As noted in the literature [14], the absorption band of NaA in between 1600 and 3700 cm^{-1} suggests the presence of zeolite water. In this case, it is dominated by a peak at 3360 cm^{-1}. This signal is associated with the H–O–H stretching (v_1 y v_3) of adsorbed water. Also, the peak at 1647 cm^{-1} could be attributed to H–O–H bending of adsorbed water (v_2).

For this zeolite type, the strong peak at about 993 cm^{-1} is associated with Si–O–Al asymmetric stretching (v_3). The absorption band at 553 cm^{-1} evidences the presence of double four-rings, and the bands appearing at 462 cm^{-1} and 669 cm^{-1} correspond to Si–O–Al bending and Si–O–Al symmetric stretching vibrations, respectively.

By comparing NaA and AgZnA spectra, the AgZnA pattern shows some changes caused by the presence of NO_3^- and NH_4^+ arising from the exchange solution. In the band corresponding to OH stretching, there is a shift of the peak from 3360 cm^{-1} to 3151 cm^{-1} with one shoulder at 3600 cm^{-1} due to the asymmetric stretching of NH_4^+ [18]. The new peak at 1400 cm^{-1} could be attributed to the asymmetric stretching of O–NO_2 overlapping with the deformation of NH_4^+ [18,19]. Also, the peak of tetrahedral internal vibrations (993 cm^{-1}) was influenced by the N–O stretching peak observed at about 1400 cm^{-1} (Fig. 2b), generating a well-defined peak at 1004 cm^{-1} [19] and a shoulder at 914 cm^{-1}. No shift of AgZnA vibrations is observed in the absorption bands representing the zeolite secondary structure (between 400 and 750 cm^{-1}). This fact provides further evidence that the framework structure remains unchanged.

3.2. Antibacterial activity of exchanged zeolites. Mic values

The antibacterial activity of AgZnA and NaA as well as their *Mic* values for *P. aeruginosa* were calculated.

Zeolite NaA did not show microbial inhibitory effects at the tested concentrations, whereas AgZnA exhibited good antimicrobial properties, as shown in Table 3 and Fig. 3.

For AgZnA in agar medium, the growth of *P. aeruginosa* diminishes with increasing Ag^{+1} and Zn^{+2} concentrations up to 200 mg·L^{-1} of AgZnA. The cell growth reduction with respect to the control medium (*P. aeruginosa* in agar without zeolite) was 75.3% for AgZnA = 50 mg·L^{-1}, 89.3% for AgZnA = 100 mg·L^{-1}, 97.2% for [Ag^{+1}] = 150 mg·L^{-1}, and 100% for AgZnA = 200 mg·L^{-1}. According to these results, no growth was obtained for [AgZnA] ≥ 200 mg·L^{-1}. Therefore, this value was defined as *Mic*. In fact, values greater than 200 mg·L^{-1} of AgZnA inhibited the production of viable cells.

Studies on the biocide capacity of Ag^{+1} ions have proposed several mechanisms of action to explain the inhibitory effect. Some researchers have reported that the positive charge of silver ion/ions is fundamental for antimicrobial activity. The electrostatic attraction between the negatively charged cell membrane and the positive charge of Ag^{+1} interferes with the permeability of the membrane [20,21]. Moreover, the mechanism of action for Zn^{+2} ions was determined to be the same as that described for Ag^{+1}. The antibacterial activity is based on the release of Zn^{+2} ions that can damage the cell membrane and interact with intracellular contents. As mentioned for silver cations, the antimicrobial activity improved with an increasing content of zinc ions [22,23].

In the particular case of *P. aeruginosa*, some studies showed that Zn^{+2} stimulates protein synthesis in these bacteria, invalidating its biocidal properties [24,25]. However, other research studies assessing the toxicity of metals showed differences in metal resistance profiles between environmental strains and hospital strains [26,27]. Most of the cases where strains showed strong resistance to antibiotics were the least resistant to metals, with the inverse also being true. However, none of the strains, irrespective of their origin, were able to grow with a supplement of 50 mM of Zn^{+2}. It was also found that multiresistance

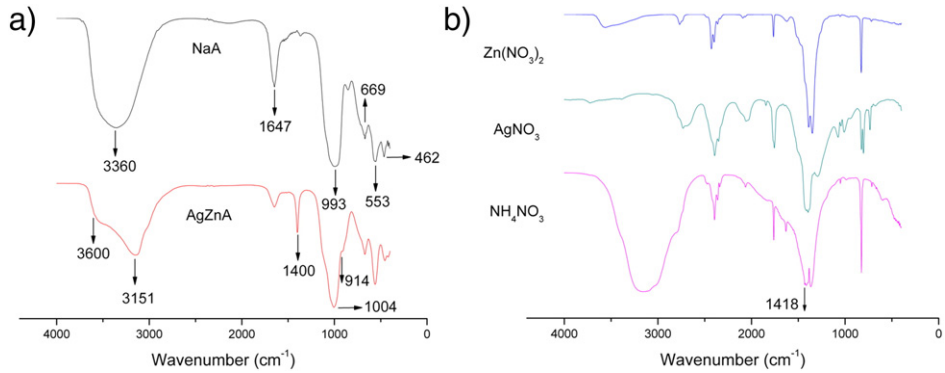

Fig. 2. FTIR spectra corresponding to a) original NaA, exchanged AgZnA, and b) nitrate salts used for ion-exchange experiments.

has been described as being widespread among environmental strains isolated from hydrocarbon-contaminated sites [27].

In the present study, it is worthwhile to think that the antibacterial activity of the Ag^{+1} and Zn^{+2} cations could depend on their location inside the zeolitic cages. In the original NaA, there are twelve sodium ions occupying three different positions or sites, denominated I, II and III. Eight sodium ions are located at site I, near the center of the six-rings inside of the alpha cage; the remaining four ions are located in the eight-rings or in the four-rings [28]. If all the sodium ions were replaced by silver ions, the chemical analysis of the zeolite should indicate a Ag content near 40 wt.%. Similarly, in the case of zinc exchange, the result of a complete replacement of sodium by zinc should indicate a 16 wt.% Zn. For the compositional analysis obtained (Table 1), not more than six of the twelve Na^{+1} ions were replaced by either Ag^{+1} or Zn^{+2}. Thus, the exchanged cations are mainly situated at site I, the most accessible site for the location of cations. Then, metallic ions occupying the exchange positions are equally accessible, and could be electrostatically attracted by the cell and subsequently released from the inorganic aluminosilicate framework. The obtained biocidal activity results suggest that the metal ions hosted in the zeolite structure were free to interact with the cell, disrupting the biochemical activity and causing cell death.

3.3. Coating analysis

3.3.1. SEM analysis

Modified epoxy coatings and coating without zeolite were studied by SEM images showing surface morphology and internal microstructure. For all the coatings, the surface image shows a smooth and homogeneous morphology, with no discontinuities or cracks in the film. In the case of epoxy modified with AgZnA, no zeolite crystals were observed on the surface, indicating that they were primarily embedded in the epoxy matrix (Fig. 4a). When studying a cross section of the film, cubic AgZnA crystals distributed into the epoxy matrix could be observed (Fig. 4b and c).

Table 3
AgZnA antibacterial activity.

AgZnA, mg·L^{-1}	Ag, mmol·L^{-1}	Zn, mmol·L^{-1}	Cell quantification, cell·mL^{-1}		
			Mean value in triplicate	Control, mean value	Antibacterial activity[a], %
50	0.025	0.046	1.0×10^7		75.3
100	0.050	0.091	4.5×10^6		89.3
150	0.075	0.138	1.2×10^6		97.2
200	0.100	0.182	0		100
				4.2×10^7	
500	0.25	0.455	0		100

[a] $100 - (CFU_{AgZnA} / CFU_{control}) \times 100$.

3.4. FTIR analysis

Fig. 5 shows the FTIR analysis of the AgZnA, epoxy polyamide cured coating and the epoxy polyamide coating modified with zeolite (4% and 8%). This analysis is commonly used to follow the reaction during the curing process [29]. The intensity of the epoxy ring vibration band at 917 cm^{-1} decreases during the curing cycle because in the final step of the reaction the epoxy rings are completely open. Simultaneously with the advance of the reaction, the intensity of the N–H band (3400–3500 cm^{-1}) diminishes while the intensity of OH bands at 3200–3500 cm^{-1} increases [30].

For the epoxy polyamide coatings modified with zeolite, the spectra obtained after curing showed the characteristic bands of this type of coating. The absorption band at 1244 cm^{-1} and the small peak at 908 cm^{-1} correspond to symmetric and asymmetric stretching of ether groups (C–O–C), respectively. Another epoxy ring peak is present at 829 cm^{-1} overlapping with the amide linkage [31]. The presence of the peak at 1244 cm^{-1} in the spectrum of epoxy coating modified with AgZnA clearly indicates that the epoxy group remains unaltered after zeolite incorporation.

A slight shift is evidenced for the peaks between 2858 and 2924 cm^{-1}, which correspond to the stretching of the CH, CH_2 and CH_3 groups.

The broad peak in the range 3500–3300 cm^{-1}, which is associated with the hydroxyl group generated from oxirane ring opening and for NH_2 and NH stretching in the epoxy coating, confirms that the curing cycle was completed [32]. In the epoxy polyamide coatings modified with zeolite, the peak was slightly shifted from 3417 cm^{-1} to 3315 cm^{-1}, probably affected by the asymmetric stretching of NH_4^+ contained in the zeolite.

The stretching band of aromatic C=C, attributed to benzene rings, is observed at 1508 cm^{-1}. The peak at 570 cm^{-1} is associated with CH groups and the peaks at 1041 cm^{-1} and 1183 cm^{-1} correspond to asymmetric and symmetric stretching of CH groups of aromatic rings.

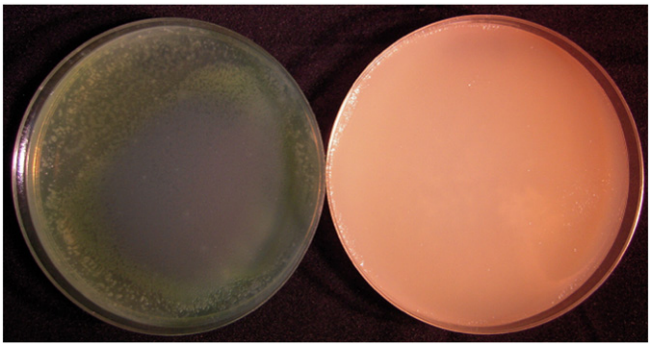

Fig. 3. Left. *P. aeruginosa* control +. Right. *P. aeruginosa* + 200 mg·L^{-1} AgZnA.

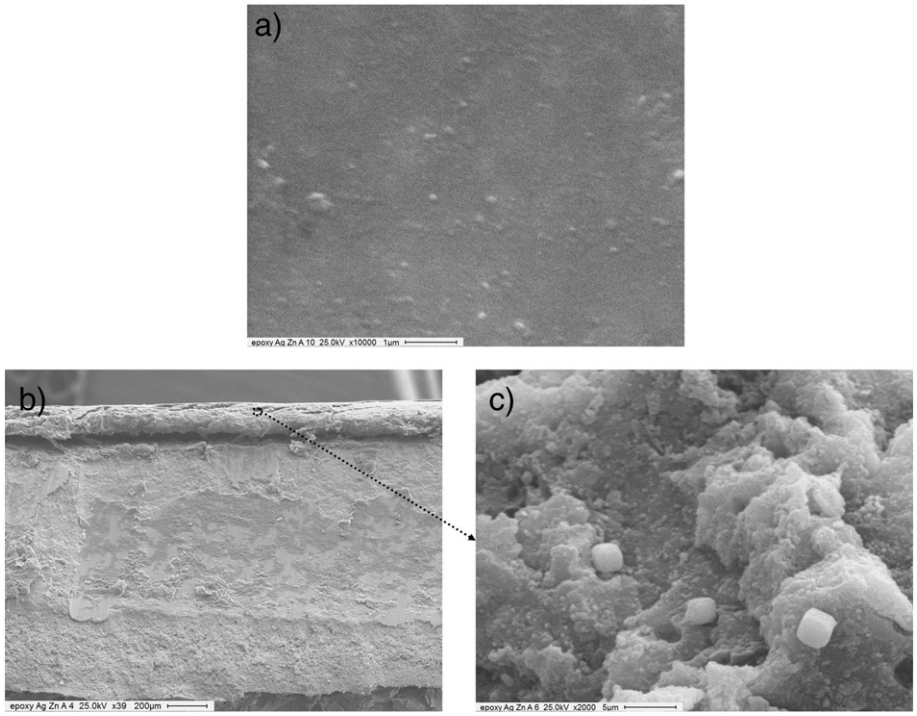

Fig. 4. SEM micrographs of the AgZnA-modified epoxy coating corresponding to V-E sample. a) Coated surface ×10,000, bar = 1 μm; b) coated coupon cross section × 39, bar = 200 μm; c) coating cross section ×2000, bar = 5 μm.

With respect to the pseudo-lattice vibrations of zeolite structural units, the peak associated with Si–O–Si stretching vibration at around 1000 cm^{-1} appears in the spectrum of epoxy coating modified with zeolite. This band does not vary during polymerization because the cages of zeolite do not break in the reaction. The incorporation of AgZnA in the epoxy coating did not introduce any new peaks in the spectra but did slightly influence the location of some of the characteristic peaks. This fact suggests an interaction between the epoxy matrix and AgZnA. Nevertheless, the positions of the absorption bands corresponding to the coating containing different AgZnA percentages were coincident

3.5. Microbiological corrosion assay in film epoxy coatings. Biomass growth

Cell quantification was performed by the technique of the most probable number (MPN) on the biofilm removed from the substrate. As shown in Table 4, the microbiological study of the biofilm detached from the coated coupon surfaces demonstrated that *P. aeruginosa* cells contained in the biofilm significantly decreased as the silver and zinc cation concentration was increased. The MPN technique applied to the biofilm allowed the observation of a significant inhibitory effect of up to seven orders of magnitude relative to the control coupon (without zeolite addition). It is important to note that zeolite matrices having different levels of biocidal cations could be obtained at the laboratory by modifying the experimental conditions used for the cation exchange step. Thus, cation contents in the coating could be varied not only by varying the zeolite weight added to the coating formulation but also by addition of the same weight of zeolite materials differing in their cation replacement level. For the AgZnA minimum concentration coupon (1%, B) no biocidal activity was detected as *P. aeruginosa* growth was identical to that of the control coating.

Simultaneously, for the cation concentration values used, the presence of Ag^{+1} and/or Zn^{+2} in the epoxy coatings does not promote the formation of inhibition zones, because no halo developed around the coupons. According to the literature [12,13], the antibacterial mechanism would take place through the absorption of cations by the bacteria, causing a disorder in the adenosine triphosphate process (ATP) and in the cell membrane. Then, the lack of inhibition zones suggests that, at the cation concentrations used in this study, cation leaching from the coated coupons did not occur and the mechanism of inhibition should be exerted via a direct contact of the epoxy coating with the bacterial cells.

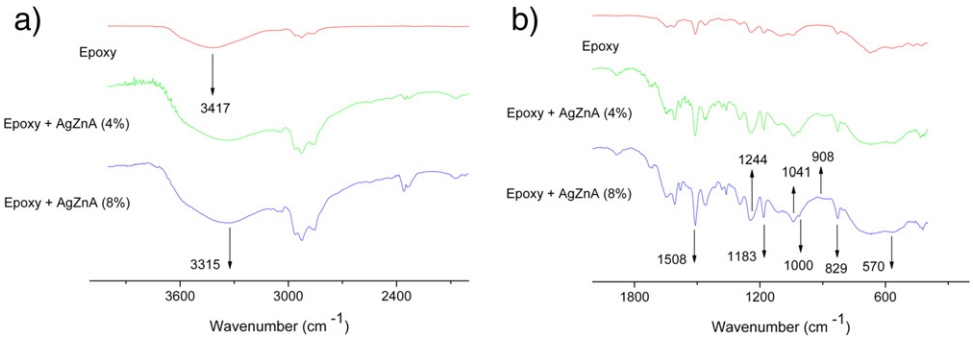

Fig. 5. FTIR patterns of epoxy coatings containing different percentages of AgZnA.

Table 4
P. aeruginosa growth in coated coupons.

Coupon-coating	*P. aeruginosa*, NMP·cm^{-2}
I-A	$>2.2 \times 10^{11}$
II-B	$>2.2 \times 10^{11}$
III-C	9.9×10^{8}
IV-D	2.8×10^{8}
V-E	3.6×10^{4}

4. Conclusions

XRD and FTIR studies showed that the incorporation of NH_4^{+1}, Ag^{+1} and Zn^{+2} in zeolite type A at the tested concentration did not promote structural modifications, with only a slight loss of crystallinity occurring. The NaA zeolite exchanged with Ag^{+1} and Zn^{+2} inhibited the growth of *P. aeruginosa* for concentrations up to 200 mg·L^{-1}. The incorporation of AgZnA into the epoxy matrix at the tested concentrations did not generate changes in the morphological aspect of the coatings and did not modify its FTIR spectral parameters, maintaining the structural order unaltered.

The addition of AgZnA to the epoxy matrix contributes to the reduction of the number of bacteria adhered to the coating. This fact involves a decrease of corrosive action caused by *P. aeruginosa* bacteria because it could minimize the different reasons leading to corrosion: the production of metabolic substances excreted such as corrosive organic acids or biosurfactants responsible for the formation of emulsions in storage tanks, the occurrence of pitting corrosion in areas where the protective coating was broken, the generation of an oxygen-free environment for sulfate-reducing bacteria host, etc.

Acknowledgments

The authors gratefully acknowledge the financial support from the FONCyT (PICT 2012-2421), UTN (PID 25/I050) and CONICET (PIP N° 112.201101-00270). The authors would also like to thank Lic A. Ermily for assistance during synthesis tests.

References

[1] H.A. Videla, Manual of Biocorrosion, Prevention, Control and Mitigation, CRC Lewis Publishers, Boca Raton, FLA, 1996. 221–240.
[2] H.A. Videla, Int. Biodeterior. Biodegrad. 49 (2002) 259–270.
[3] D. Allshop, K. Seal, C. Gaylarde, Introduction to Biodeteroration, Cambridge University Press, USA, 2004. 44–53.
[4] A.C. Rouw, Prog. Org. Coat. 34 (1998) 181–192.
[5] M.H. Ifran, Chemistry and Technology of Thermosetting Polymers in Construction Applications, Springer, Germany, 1998. 78.
[6] T. Haile, G. Nakla, Biofouling 25 (2009) 1–12.
[7] D. Boschetto, I. Lerin, R. Cansian, S. Castellã Pergher, M. Di Luccio, Chem. Eng. J. 204–206 (2012) 210–216.
[8] S. Bedi, R. Cai, C. O'Neill, D.E. Beving, S. Foster, S. Guthrie, W.S. Chen, Y. Yan, Microporous Mesoporous Mater. 151 (2012) 352–357.
[9] P. Kaali, E. Strömberg, R.E. Aune, G. Czél, D. Momcilovic, S. Karlsson, Polym. Degrad. Stab. 95 (2010) 1456–1465.
[10] G. Cerri, M. De Gennaro, M.C. Bonferoni, C. Caramella, Appl. Clay Sci. 7 (2004) 141–150.
[11] W. De Muynck, N. De Belle, W. Verstraete, Cement Concr. Compos. 31 (2009) 163–170.
[12] T. Haile, G. Nakhla, E. Allouche, S. Vaidya, Corros. Sci. 52 (2010) 45–53.
[13] T. Haile, G. Nakhia, Geomicrobiol J. 25 (2008) 322–331.
[14] W.D. Breck, Zeolite Molecular Sieves, Wiley, New York, 1974.
[15] 1998.
[16] O.L. Corona, M.A. Hernández, F. Hernandez, F. Rojas, R. Portillo, V.H. Lara, F.M. Carlos, Matéria (Rio de Janeiro) 14 (3) (2009) 918–931.
[17] P. Castaldi, L. Santona, C. Cozza, V. Giuliano, C. Abbruzzese, V. Nastro, P. Melis, J. Mol. Struct. 734 (2005) 99–105.
[18] G.J. Boer, I.N. Sokolik, S.T. Martin, J. Quant. Spectrosc. Radiat. Transf. 108 (2007) 17–38.
[19] T. Biswick, W. Jones, A. Pacula, E. Serwicka, J. Solid State Chem. 179 (2006) 49–55.
[20] P. Dibrov, J. Dzioba, K.K. Gosink, C. Häse, Antimicrob. Agents Chemother. 46 (2002) 2668–2670.
[21] J.S. Kim, E. Kuk, K. Nam Yu, J. Kim, S.J. Park, H.J. Lee, S.H. Kim, Y.K. Park, Y.H. Park, C.Y. Hwang, Y.K. Kim, Y.S. Lee, D.H. Jeong, M.H. Cho, Nanomed. Nanotechnol. 3 (2007) 95–101.
[22] X. Wang, Y. Du, H. Liu, Carbohydr. Polym. 56 (2004) 21–26.
[23] R. Brayner, R. Ferrari-Iliou, N. Brivois, S. Djediat, M.F. Benedetti, F. Fievet, Nano Lett. 6 (2006) 866–870.
[24] A. Hassen, N. Saidi, M. Cherif, A. Boudabous, Bioresour. Technol. 65 (1998) 873–882.
[25] G. Özdemir, M. Hoşgör Limoncu, S. Yapar, Appl. Clay Sci. 48 (2010) 319–323.
[26] A. Top, S. Ülkü, Appl. Clay Sci. 27 (2004) 13–19.
[27] A. Deredjian, C. Colinon, E. Brothier, S. Favre-Bonté, B. Cournoyer, S. Nazaret, Res. Microbiol. 162 (2011) 689–700.
[28] R. Szostak, Handbook of Molecular Sieves, Van Nostrand Reinhold, New York, 1992. 258.
[29] C. Ramírez, M. Rico, A. Torres, L. Barral, J. López, B. Montero, Eur. Polym. J. 44 (2008) 3035–3045.
[30] J. González-Benito, J. Colloid Interface Sci. 267 (2003) 326–332.
[31] M. Selvaraj, K. Maruthan, G. Venkatachari, Corros. Sci. 48 (2006) 4365–4377.
[32] E. Huttunen-Saarivirta, G.V. Vaganov, V.E. Yudin, J. Vuorinen, Prog. Org. Coat. 76 (2013) 757–767.